Journal of Alloys and Compounds 691 (2017) 1–7

Contents lists available at ScienceDirect

Journal of Alloys and Compounds

journal homepage: http://www.elsevier.com/locate/jalcom

Structural and magnetic properties of Fe_3Ga alloy nanowires: Effect of post annealing treatment

Muhammad Irfan [a], U. Khan [a], Wenjing Li [a], Wenjie Kong [a], K. Javed [b], X.F. Han [a, *]

[a] Beijing National Laboratory for Condensed Matter Physics, Institute of Physics, Chinese Academy of Sciences, Beijing, 100190, China
[b] Department of Physics Forman Christian College Lahore, 5400, Pakistan

ARTICLE INFO

Article history:
Received 4 July 2016
Received in revised form
17 August 2016
Accepted 23 August 2016
Available online 25 August 2016

Keywords:
Electrodeposition
Nanowires
STEM-EDX
Annealing treatment
Magnetic response

ABSTRACT

We report on the influence of the annealing temperature on the crystal structure phase change, effective anisotropy energy and magnetization reversal of electrodeposited Fe_3Ga nanowires (NWs) with diameter of 80 nm. Scanning transmission electron microscopy (STEM) energy-dispersive X-ray (EDX) spectroscopy technique for the elemental mapping of Fe_3Ga NWs showed clearly the homogeneous distribution of Fe and Ga. These NWs are highly aligned to each other and exhibits high geometrical aspect ratio. The crystal structure of these nanowires shows strong dependence on the sintering temperature. X-ray diffraction reflects the highly textured A2-disorderd phase with precipitates of DO_3 and $L1_2$ phase for as-synthesized Fe_3Ga NWs. As the annealing temperature increases, the intensity of strong disordered phase A2 or short range order phase DO_3 suddenly decreases and grains are textured along the stable $L1_2$ phase with small precipitates of DO_3 phase. As a result of these structural changes, magnetization reversal mode switches from transverse to a combination of transverse and vortex modes. Angular magnetic response at room temperature is employed to identify the magnetization reversal modes for Fe_3Ga NWs. Temperature dependent coercivity response can be understood in terms of thermal activation over an energy barrier with a $\frac{3}{2}-$ power dependence on the field.

1. Introduction

It is well known that nowadays magnetic NW arrays have received considerable attention due to potential applications in the field of sensors, data storage media, sensors, actuators, etc [1–7]. The accurate measurement of the magnetic properties of nanostructures is highly important. The magnetic response in magnetic nanostructures is highly dependent upon their dimensional configuration like as shape, size, aspect ratio and spacing between adjacent elements [8]. It has been reported in many research articles that the materials possessing magnetic property of magnetostriction are of interest in energy harvesters, actuators, and sensors [9]. Large magnetic field which induces strains approximately 2k-ppm has been achieved in Terfenol-D which is considered a material with large magnetostrictive property [10]. Alloys based on FeGa (Galfenol) are promising candidates due to their several advantages like low saturation magnetic field, large tetragonal magnetostrictive coefficient, low cost and excellent ductility [11–14]. It is well-known that composition, annealing history and synthesis routes have been accused for magnetic response of Fe based alloys and compounds [15]. Furthermore, magnetic nanowires, due to their low dimensionality becomes of particular interest as compared with their bulk properties in the field of electronics, optics, semi-conductors, and magnetism [16]. The aim of present work is to report fabrication with their structural and magnetic characterizations of Fe_3Ga nanowires that are grown by the electrodeposition technique.

2. Experimental details

Fe_3Ga nanowires were fabricated by electrodeposition using AAO templates with pore size of 80 nm. Before electrodeposition process, the shining side of AAO template was coated with a copper layer thickness of 200 nm as the working electrode for reduction of Fe and Ga ions from the electrolyte. A small strip of 0.2 mm thick Pt sheet was used to serve as a counter electrode. The electrolyte was consisted of 0.1 g/50 ml $FeSO_4$, 0.5 g/50 ml $Ga_2(SO_4)_3$, 0.3 g/50 sodium citrate and 0.01 g/50 ml L-ascorbic acid in deionized water. The electrodeposition was carried out under constant magnetic stirring,

* Corresponding author.
E-mail address: xfhan@iphy.ac.cn (X.F. Han).

http://dx.doi.org/10.1016/j.jallcom.2016.08.241
0925-8388/

and at a biasing voltage of −1.2 V (versus SCE). The NWs of Fe_3Ga grew in the usual bottom-up way starting from the Cu electrode at the pore bottoms of AAO template. After deposition, the magnetic NWs were annealed at temperatures 550 °C, 600 °C and 650 °C. The samples were designated as T1-As-synthesized, T2-annealed at 550 °C, T3-annealed at 600 °C and T4-annealed at 650 °C.

The samples were micro-structurally analyzed by X-ray diffraction (XRD: RIGAKU-D/MAX-2400, Cu Kα, λ = 0.154056 nm). The detailed morphology of NWs was collected by Field Emission Scanning Electron Microscopy (FE-SEM: Hitachi S-4800) and compositional analysis were characterized with Energy Dispersive X-ray spectroscopy (EDS) integrated with FE-SEM. (TEM) transmission electron microscopy (TEM: TecnaiF20). Magnetic measurements were performed by magnetic sample magnetometer (VSM: Microsense EV-9) and physical property measurement system (PPMS-model, 9 T).

3. Results and discussion

Unique anodic aluminum oxide (AAO) templates with self-assembled hexagonally arranged nanopores are ideal for synthesis of nanoscale materials due to easy preparation and controllable pore size. Here, porous alumina membranes with pore diameter of 80 nm is used to fabricate the Fe_3Ga NWs. Fig. 1 depicts the schematic diagram of the synthesis process of Fe_3Ga nanowires within the pores of AAO-template via electrodeposition method in detail. First, the shining side of AAO membrane is sputtered with Cu (200 nm), then NWs were grown through electrochemical rout. Afterwards, the template filled with NWs were chemically etched with NaOH etchant (partially) for 30 min at 60 °C and (complete) 24 h at 60 °C for FE-SEM and TEM measurements respectively, (Fig. 1). Fig. 2 shows the morphology of Fe_3Ga NWs characterized by using a field emission scanning electron microscope (FE-SEM) and a transmission electron microscope (TEM). The diameters for all of the NWs are consistent with the diameters of the AAO channel. It is apparent from Fig. 2 (a–b) that Fe_3Ga NWs were grown in highly uniform fashion. The length of these crack free and smooth NWs extends to several μm that can be seen in Fig. 2 (c) and inset of Fig. 2 (d). The elemental contribution of Fe and Ga in FeGa-alloy system of NWs is shown in Fig. 2 (d). This confirms the existence of Fe and Ga in the required ratio of (3:1) respectively. It should be pointed out that some other elements are also present besides Fe, and Ga in the spectrum due to incomplete etching and Au sputtering before SEM measurement. Furthermore, STEM-EDX elemental mapping of Fe_3Ga nanowire showing clearly the homogeneous distribution of Fe and Ga in Fig. 3.

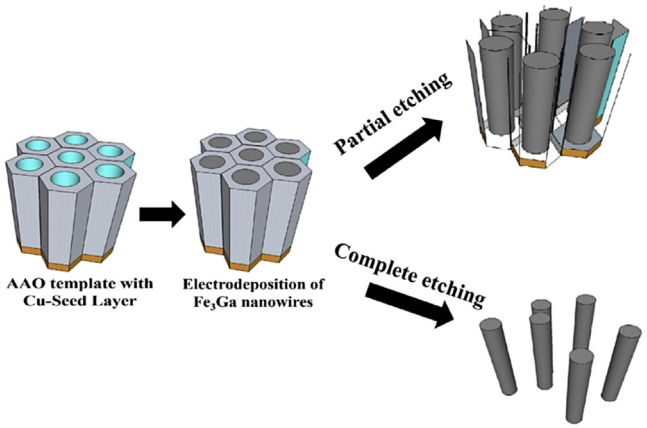

Fig. 1. Complete fabrication procedure of Fe_3Ga nanowires.

The XRD patterns of as-synthesized and post annealed nanowires are shown in Fig. 4. Only three strong peaks were observed from as-synthesized sample at ~42.6°, ~43.6° and ~80.8° corresponding to (111), (110) and (211) reflections originating $L1_2$ and A2 structures. Since Fe_3Ga is most likely crystal structure with possibility for DO_3 crystal phase and have X-ray reflections at (220) and (422) at 43.6° and 80.8°, respectively, since the alloy composition is $Fe_{75}Ga_{25}$. The number of diffraction peaks changed with annealing temperature. At temperature T2, the $L1_2$ structure is partially dominant along with DO_3 phase. As the temperature increases to T3, the intensity of strong disordered phase A2 or order phase DO_3 suddenly decreases and grains are textured along the stable $L1_2$ phase with small precipitates of DO3 phase. At higher temperature T4, the disorder phase along (110) and (211) again start to develop along the stable phase. From Fig. 4, we have the intensity ratio (I_{211}/I_{110} or I_{422}/I_{220}) = 0.247, 0.264 and 0.434 respectively for T1, T2 and T4 which depicts that Fe_3Ga is highly (110) or (220) textured for T1 and T2. For randomly oriented Fe powder, the intensity ratios of highly texture reflections are: $I_{200}/I_{110} = 0.50$ and $I_{211}/I_{110} = 0.80$ [17].

The grain size, D, can be estimated from the broadness of the diffraction peak using Debye–Scherer's relationship given by

$$D = \frac{k\lambda}{LCos\theta} \quad (1)$$

where λ is the wavelength of the Cu-Kα radiation, θ is the diffraction angle of highly textured/intensity reflection, k is the Scherer's constant which takes the value of 0.89 for spherical crystals with cubic symmetry [18,19] and L is the FWHM of the diffraction line corrected for the instrumental broadening. The grain size collected for as synthesized and post annealed nanowires are 31 nm, 27 nm, 40 nm and 44 nm respectively. This behavior is attributed to the recrystallization phenomena of grains and transformation from the disorder to the stable phase with raising of annealing temperature. Smaller crystallites are thermodynamically less stable than larger ones due to their high surface energy. Accordingly, they recrystallize such as in bubble coalescence during the longer delay times to attain more stable bigger crystallites [20].

We observed a non-hysteretic behavior for θ = 90°. This trend attributes that the shape anisotropy of Fe_3Ga NWs may induce a hard axis of magnetization for θ = 90° and is shown in Fig. 5. There are two stable orientations of magnetic moments that are directed parallel and perpendicular to the wire long axis. The slightly hysteretic nature for perpendicular measurement may be the effect of rather weak magneto-crystalline anisotropy. The magnetic spins are easily aligned along the magnetic field direction, so we get the squared hysteresis loop and high values of coercivity in comparison with coercivity and slightly hysteretic nature when field is applied perpendicular to the NWs axis. Fig. 5 reflects that the in-plane coercivity values enhancing with annealing treatment and attains maxima for stable $L1_2$ phase of Fe_3Ga alloy. It also clears that NWs having the mixed highly disorder (A2)/order (DO_3) phase have the low coercivity values as compared to the highly textured $L1_2$ phase. The gradual approach to saturation of the curve measured with the perpendicular field is an indication of magnetization rotation process. The angular hysteresis loops for as-synthesized nanowires shown in Fig. 6 also demonstrate that the value of saturation field increases from θ = 0° to θ = 90°. This behavior is typical of the systems with uniaxial anisotropy.

Fig. 7 elucidates that easy axis is parallel to the NWs long axis (highest values of SQ are at θ = 0°) for all the samples under investigation. Conventionally, the sign of the saturation fields difference $\Delta H_s = (H_s)_{para} - (H_s)_{perp}$ gives the idea about the easy magnetization axis in case of NWs., where $(H_s)_{para}$ and $(H_s)_{perp}$ are

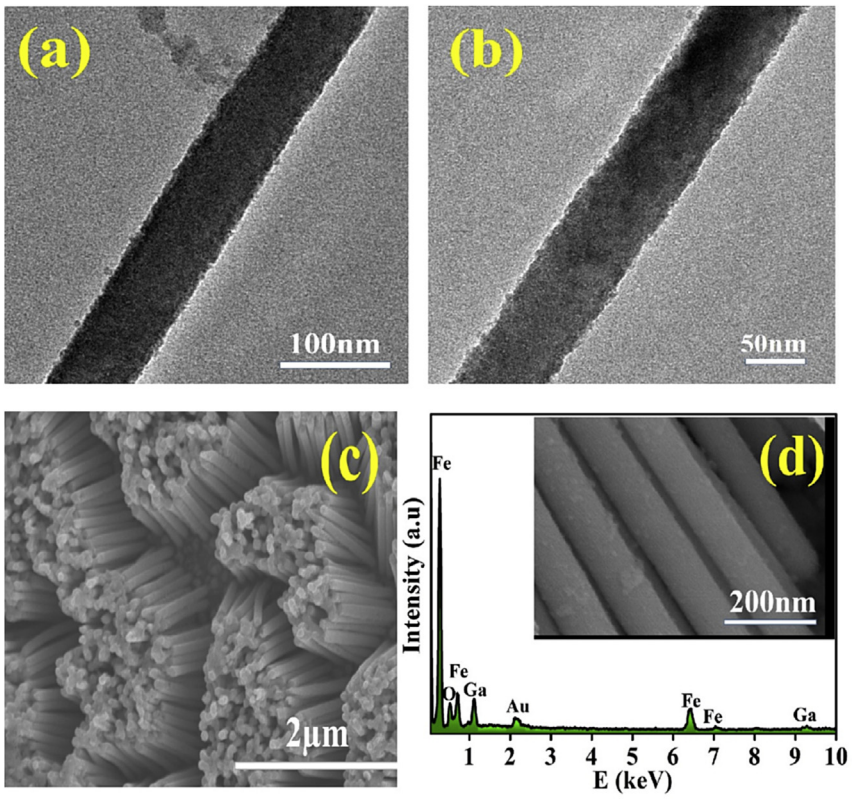

Fig. 2. Characterizations of Fe_3Ga nanowires after complete/partially removing the AAO template. (a–b) TEM images with different magnifications, scale bars are 100 and 50 nm, respectively. (c–d) High-magnification SEM images and EDX-spectra of Fe_3Ga nanowires.

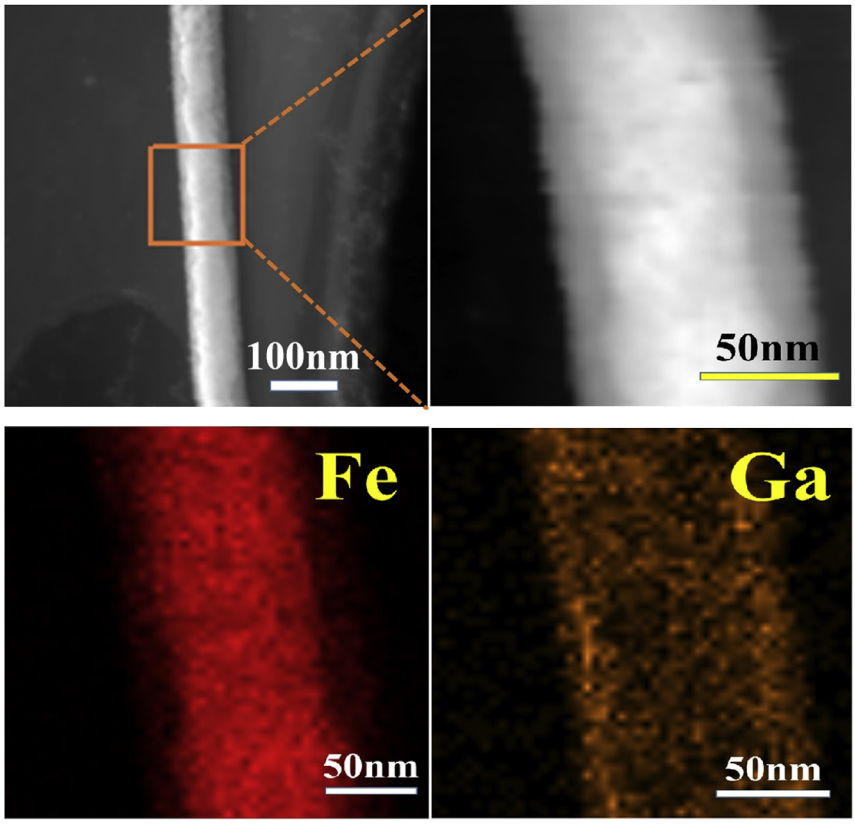

Fig. 3. STEM-EDX elemental mapping of Fe_3Ga nanowire showing clearly the homogeneous distribution of Fe and Ga.

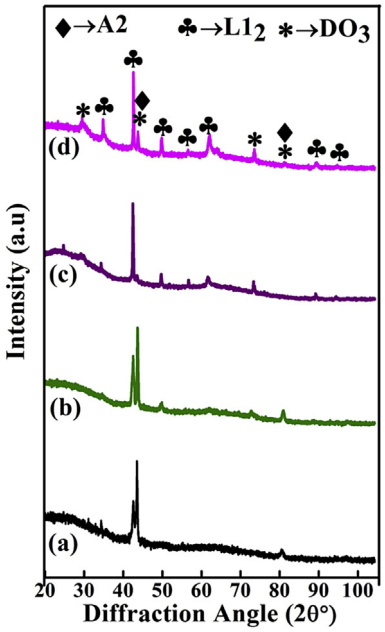

Fig. 4. XRD spectra for Fe_3Ga nanowires annealed at (a) room temperature, (b) at 550 °C, (c) at 600 °C and (d) at 650 °C.

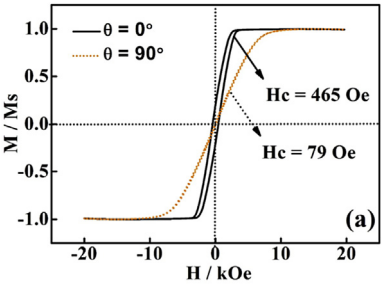

Fig. 5. Normalized longitudinal and perpendicular hysteresis loops for (a) as-synthesized and (b–d) post annealed Fe_3Ga nanowires.

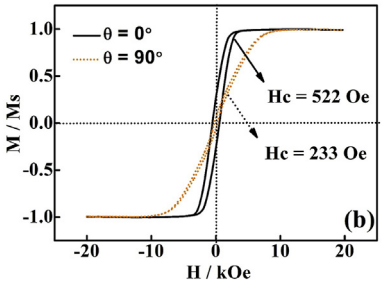

Fig. 5. (*continued*).

the saturation fields values for magnetic field applied parallel and perpendicular to the NWs axis, respectively. The negative sign of ΔH_s dictates that easy axis is parallel to the wire long axis and positive sign gives the signal for easy axis perpendicular to the wire long axis. In our case, Fig. 5 shows that the saturation field is higher for $\theta = 90°$ than the saturation field for $\theta = 0°$, so the negative sign of ΔH_s is there which directly corresponds to easy axis parallel to the wire axis. The SQ values decrease with the increase in angle for as-synthesized and post annealed Fe_3Ga nanowires. The low SQ (Mr/Ms) ratio observed in the case of parallel field, where it is

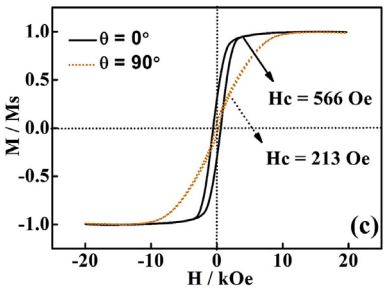

Fig. 5. (*continued*).

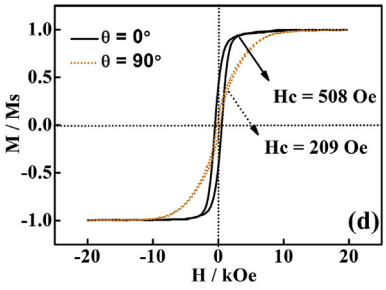

Fig. 5. (*continued*).

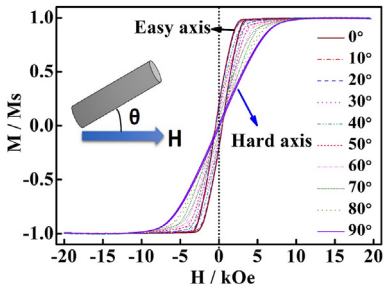

Fig. 6. Room-temperature angular dependent hysteresis loops for as-synthesized Fe_3Ga nanowires, inset shows schematic diagram for the angle between applied magnetic field and NWs during magnetic measurements.

expected to be ~1, is due to high interwire interactions.

Coercivity, field required to demagnetize the materials is an important property especially in ferromagnetic materials and understanding of it can provide insight into magnetization reversal processes. In case of magnetic NWs, the magnetization reversal process and magnetic coercivity readily change with the angle between the field and NWs axes. Therefore, the angular response of coercivity is directly correlated to the magnetization reversal. To get insights for reversal modes in Fe_3Ga nanowires, the variation of coercivity after extracting data from MH-loops is plotted as a function of angle and is shown in Fig. 8.

The most common studied magnetization reversal modes in NWs are, a) Coherent Rotation Mode (CRM), where all the magnetic spins rotate coherently, b) Localized Coherent rotation Mode (LCRM) or Transverse Mode (TM), where magnetic moments reverse progressively via propagation of a transverse domain wall, c) Curling Mode (CM), where all the magnetic moments curl simultaneously, d) Localized curling Mode (LCM) or Vortex Mode (VM), where magnetic moments reverse progressively via propagation of a vortex domain wall. Variation of coercivity (Hc) with the applied field angle gives the knowledge about the working modes during reversal process [21]. For CRM and TM, Hc values decrease

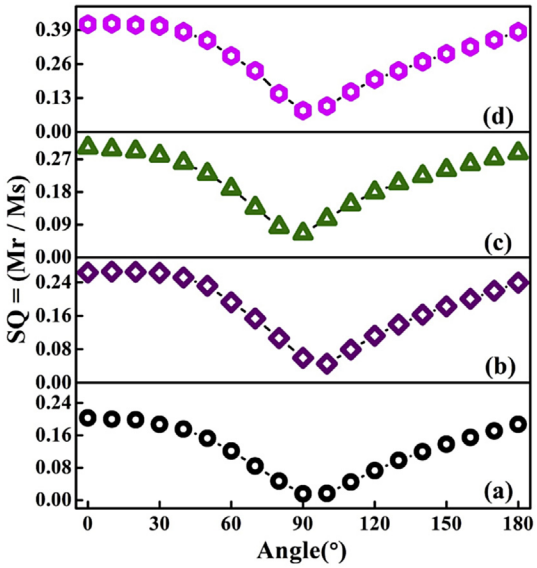

Fig. 7. Angular dependent of SQ for (a) as-synthesized and (b–d) post annealed Fe_3Ga nanowires.

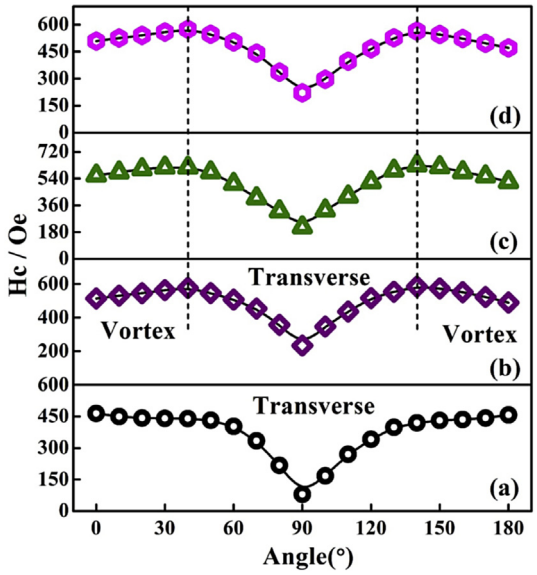

Fig. 8. Angular dependent of coercivity for (a) as-synthesized and (b–d) post annealed Fe_3Ga nanowires.

with applied field angles in the $0^\circ - 90^\circ$ ranges and attain minimum at $\theta = 90^\circ$, whereas in CM and VM, the Hc values increase continuously giving peak at $\theta = 90^\circ$ angle. It was pointed out that CRM is only favorable for magnetic nanostructures whose length is comparable with domain wall width. Fig. 8 displays the experimental findings of H_c (θ) for as-synthesized and post annealed Fe_3Ga nanowire arrays respectively. The value of H_c (θ) is found to be monotonic decrease with the applied field angle in case of as-synthesize nanowires: so we can observe the transverse reversal mode of magnetization as a function of θ. Non-monotonic behavior of angular coercivity in case of post annealed nanowires is observed: it continuously increased from 0° to 40° and then decreased in the range $40^\circ < \theta < 90^\circ$, thus indicating a switching mechanism in magnetization reversal process depending on applied field angle. There is a characteristic peak around 40° in the coercivity plots below which the mode of reversal is VM and above is TM. Low value of saturation magnetization or decreasing trend of shape anisotropy may be responsible for the decreasing behavior of Hc value in the low angular range [22]. In high angular range, H_c of nanostructure approached zero at $\theta = 90^\circ$, it can be expected theoretically for an infinitely long cylinder. Many researchers [23–25] have also been reported M-type fashion of angular response of coercivity on magnetic NWs.

Effective anisotropic energy $\boldsymbol{K_{eff}}$ plays key role for NWs in magnetic recording media. The effective anisotropy energy, $\boldsymbol{K_{eff}}$ has been evaluated from the experimental magnetization loops using the relation [26]:

$$\boldsymbol{K_{eff} = 2\pi M_s \left[(H_s)_{para} - (H_s)_{perp} \right]} \quad (2)$$

The behavior of effective anisotropy is shown in Fig. 9. It can be seen that the value of $\boldsymbol{K_{eff}}$ being reduce with enhancing the annealing temperature for Fe_3Ga nanowires. This trend shows the low values saturation magnetization with increasing the annealing temperature of nanowires [23]. In all of our cases $\boldsymbol{K_{eff} > 0}$, the easy axis of magnetization is along the wire axis. This behavior can be interpreted by taking into account all the anisotropies present in the NW arrays. The main contributions to the effective anisotropy field $\boldsymbol{H_{eff}}$ are (a) *shape anisotropy*, the field that induces a magnetic easy axis parallel to the wire's long axis; (2) *dipole-dipole interactions*, the field that tries to rotate the easy axis perpendicular to the NWs; and (3) *magneto crystalline anisotropy field* $\boldsymbol{H_k}$. Taking three factors into considerations, the effective anisotropy energy $\boldsymbol{K_{eff}}$ can be defined as follows [27]:

$$\boldsymbol{K_{eff} = \pi M_s^2 (1 - 3P) + K_1} \quad (3)$$

where P is the porosity of nanowire array determined by $\boldsymbol{P = \frac{\pi}{2\sqrt{3}} \frac{d^2}{R^2}}$ (R is interwire distance and d is wire diameter), $\boldsymbol{\pi M_s^2}$ is the shape demagnetization energy, $\boldsymbol{-3p\pi M_s^2}$ correspond to dipolar energy and $\boldsymbol{K_1}$ is the magneto crystalline anisotropy energy. In our case shape anisotropy is dominant to orient the moments parallel to the wire axis but the low value of squarness (field applied easy axis direction) also designates the role of dipolar interaction energy. Fig. 9 (inset) displays that the inter-pore distance in the alumina template is ~d = 125 nm. The high pore density or low inter-pore for AAO-template results in high interwire interactions which directly induce a dipolar field. AAO-template is not able to mediate exchange interactions over more than a few interatomic distances, so the only source of interaction between NWs is through magneto static dipolar interactions.

Temperature induces a dynamic magnetization reversal in magnetic nanowire arrays. Therefore, understanding the impact of

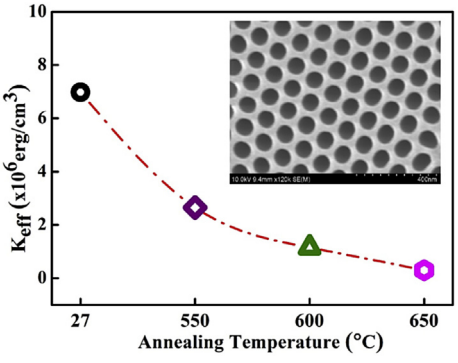

Fig. 9. Effective anisotropy energy (inset shows the FE-SEM image of AAO-template).

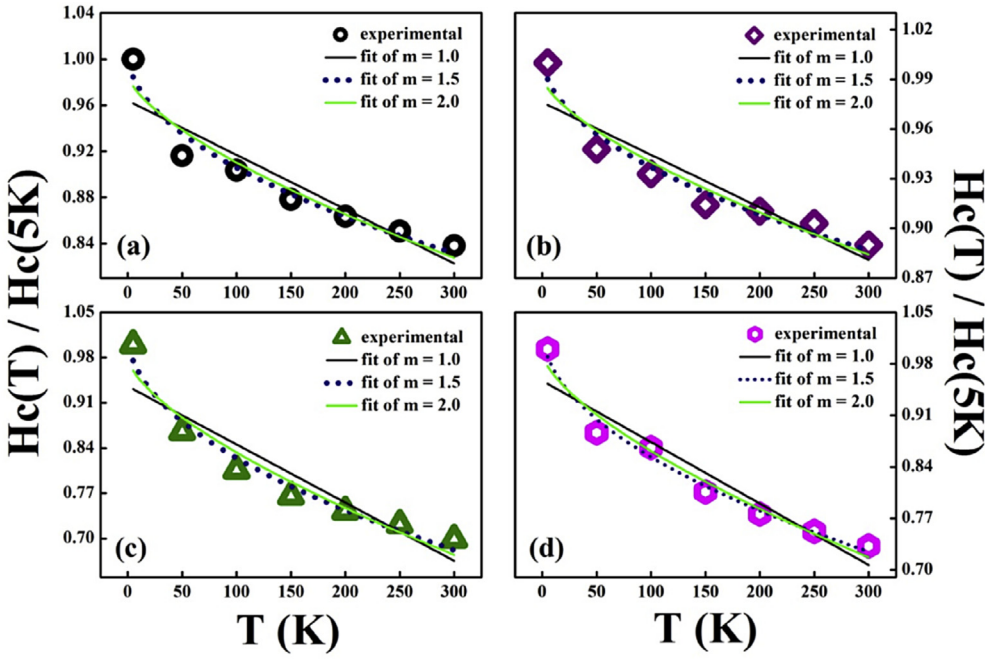

Fig. 10. Normalized coercivity as a function of temperature for Fe_3Ga nanowires annealed at (a) room temperature, (b) at 550 °C, (c) at 600 °C and (d) at 650 °C. The lines are fitting curves using Eq. (4) with m = 1, 1.5, 2 values.

temperature on the magnetic properties is important to avoid undesirable effects resulting from temperature fluctuation [20]. The behavior of Fe_3Ga nanowires can be explained by thermal activation of magnetization over a single energy barrier proposed by Brown model and temperature dependence of coercivity in this model can be given by the relationship [28].

$$H_c(T) = H_{c0}\left[1 - \frac{25Tk_B}{E}\right]^{\left(\frac{1}{m}\right)} \quad (4)$$

where H_{c0} is the switching field without thermal fluctuation, E is the barrier height in the absence of the external field, and k_B is the Boltzmann constant. Fig. 10, together with fits to Eq. (4) with m = 1, 1.5 and 2 respectively demonstrates that H_c showing increasing behavior by decreasing the temperature, obtained after measuring a series of MH-loops at different temperatures in a field of up to 1 kOe. It should be noted that increase in H_c is small from 300 to 5 K in case of as-synthesized and low temperature annealed NWs and high for rest of the samples. Since the dipolar magneto-static interactions always lower the H_c value [29], therefore very small change in H_c values from 300 to 5 K dictates the relatively weak interactions for samples T1 and T2 at 5 K. It is clearly seen that for all four samples, only the curves with $m = 1.5$ match almost every data point. Neither $m = 2$ nor 1 can fit the whole temperature range as well as $m = 1.5$. The physical origin of $\frac{3}{2}$ -power law is the non-symmetric energy landscape [28].

Finally, we have observed that due to versatile and enhanced magnetic properties of technologically important intermetallic alloys such as FeGa nanowires make them important for different applications like magnetic sensors, magnetic actuators based on magnetic NWs. This opens up enormous possibilities for fabricating nanoscale devices for a variety of applications.

4. Conclusion

Arrays of Fe_3Ga nanowires with various annealing temperature have been successfully synthesized by electrodeposition method into the pores of AAO templates. XRD analysis showed that heat treatment of nanowires developed the stable $L1_2$ phase from the order DO_3 and disorder A2 phase. We have concluded that magnetization reversal mode for Fe_3Ga NWs based on annealing temperature. Easy axes along the wires long axis depicts the major contribution of shape anisotropy. The temperature dependence of coercivity yields a $\frac{3}{2}$ power law for the field dependence of the energy barriers responsible for hysteresis.

Acknowledgements

The project was supported by the State Key Project of Fundamental Research and 863 Plan Project of Ministry of Science and Technology [MOST 2014AA032904], the MOST National Key Scientific Instrument and Equipment Development Projects [Grant No. 2011YQ120053], the National Natural Science Foundation of China [NSFC, Grant No. 11374351 and 11434014] the Strategic Priority Research Program (B) of the Chinese Academy of Sciences (CAS) [Grant No. XDB07030200].

References

[1] A. Khayatian, M.A. Kashi, R. Azimirad, S. Safa, J. Phys. D. Appl. Phys. 47 (2014) 075003–075010.
[2] S.Y. Chou, Proc. IEEE 85 (1997) 652.
[3] S.S. Ali, W.J. Li, K. Javed, D.W. Shi, S. Riaz, Y. Liu, Y.G. Zhao, G.J. Zhai, X.F. Han, Nanoscale 7 (2015) 13398.
[4] N. Adeela, K. Maaz, U. Khan, S. Karim, M. Ahmad, M. Iqbal, S. Riaz, X.F. Han, M. Maqbool, Ceram. Inter 42 (2016) 1020.
[5] M. Irfan, U. Khan, W.J. Li, N. Adeela, K. Javed, X. f. Han, Mater. Lett. 180 (2016) 235–238.
[6] U. Khan, W.J. Li, N. Adeela, M. Irfan, K. Javed, C.H. Wan, S. Riaz, X.F. Han, Nanoscale 8 (2016) 6064.
[7] U. Khan, M. Irfan, W.J. Li, N. adeela, P. Liu, Q.T. Zhang, X.F. Han, Nanoscale 8 (2016) 14956.
[8] J.J. Park, M. Reddy, B.J.H. Stadler, A.B. Flatau, J. Appl. Phys. 113 (2013) 17A331.
[9] M. Liu, S. Li, Z. Zhou, S. Beguhn, J. Lou, F. Xu, T.J. Lu, N.X. Sun, J. Appl. Phys. 112 (2012) 063917.
[10] A.E. Clark, J.B. Restorff, M.W. Fogle, T.A. Lograsso, D.L. Schlagel, IEEE Trans. Mag. 36 (2000) 3238.

[11] S. Guruswamy, N. Srisukhumbowornchai, A.E. Clark, J.B. Restorff, M.W. Fogle, Scr. Mater. 43 (2000) 239.
[12] J. Atulasimha, A.B. Flatau, Smart Mater. Struct. 20 (2011) 043001.
[13] A.E. Clark, K.B. Hathaway, M.W. Fogle, J.B. Restorff, T.A. Lograsso, V.M. Keppens, G. Petculescu, R.A. Taylor, J. Appl. Phys. 93 (2003) 8621–8623.
[14] N. Kawamiya, K. Adachi, Y. Nakamura, J. Phys. Soc. Jpn. 33 (1972) 1318.
[15] D.L.L. Pelecky, R.D. Rieke, Chem. Mater. 8 (1996) 1770.
[16] M.C. Zhang, H.L. Jiang, X.X. Gao, J. Zhu, S.Z. Zhou, J. Appl. Phys. 99 (2006) 023903.
[17] S.U. Jen, W.C. Cheng, F.L. Chiang, J. Alloys Compd. 651 (2015) 544–550.
[18] X. Zhang, H. Zhang, T. Wu, Z. Li, Z. Zhang, H. Sun, J. Magn. Magn. Mater. 331 (2013) 162–167.
[19] M. Irfan, N. A. Niaz, I. Ali, S. Nasir, A.Shakoor, A.Aziz, N.Karamat, N. R.Khalid, J. Elect. Mater. DOI: 10.1007/s11664-015-3770-0.
[20] M.S. Salem, P. Sergelius, R. Zierold, J.M.M. Moreno, D. Gorlitz, K. Nielsch, J. Mater. Chem. 22 (2012) 8549.
[21] L. Sun, Y. Hao, C.-L. Chien, P.C. Searson, IBM J. Res. Dev. 49 (2005) 79.
[22] G.C. Han, B.Y. Zong, P. Luo, Y.H. Wu, J. Appl. Phys. 93 (2003) 9202.
[23] S. Goolaup, N. Singh, A.O. Adeyeye, V. Ng, M.B.A. Jalil, Eur. Phys. J. B 44 (2005) 259.
[24] R. Lavin, J.C. Denardin, A.P. Espejo, A. Cortes, H. Gomez, J. Appl. Phys. 107 (2010) 09B504.
[25] T.N. Narayanan, M.M. Shaijumon, L. Ci, P.M. Ajayan, M.R. Anantharaman, Nano Res. 1 (2008) 465–473.
[26] K.R. Pirota, E.L. Silva, D. Zanchet, D. Navas, M. Vázquez, M.H. Vélez, M. Knobel, PRB 76 (2007) 233410.
[27] H. Yang, Y. Li, M. Zeng, W. Cao, W.E. Bailey, R. Yu, Sci. Rep. 6 (2016) 20427.
[28] H. Zeng, R. Skomski, L. Menon, Y. Liu, S. Bandyopadhyay, D.J. Sellmyer, PRB 65 (2002) 134426.
[29] R. Sharif, X.Q. Zhang, S. Shamaila, S. Riaz, L.X. Jiang, X.F. Han, J. Magn. Magn. Mater. 310 (2007) 830–832.